Title

Internode length is reduced during myelination and remyelination by neurofilament medium phosphorylation in motor axons

Authors

Villalón, Eric
Barry, Devin M
Byers, Nathan
et al.

Publication Date

2018-08-01

DOI

10.1016/j.expneurol.2018.05.009

Peer reviewed

HHS Public Access

Author manuscript

Exp Neurol. Author manuscript; available in PMC 2019 August 01.

Published in final edited form as:

Exp Neurol. 2018 August ; 306: 158–168. doi:10.1016/j.expneurol.2018.05.009.

Internode Length is Reduced During Myelination and Remyelination by Neurofilament Medium Phosphorylation in Motor Axons

Eric Villalón[1,2,*], **Devin M. Barry**[3,*], **Nathan Byers**[6], **Katie Frizzi**[5], **Maria R. Jones**[1,2], **Dan S. Landayan**[4], **Jeffrey M. Dale**[1,2], **Natalie L. Downer**[7], **Nigel A. Calcutt**[5], and **Michael L. Garcia**[1,2,†]

[1]Department of Biological Sciences, University of Missouri, Columbia, MO 65211

[2]C.S. Bond Life Sciences Center, University of Missouri, Columbia, MO 65211

[3]Department of Anesthesiology, Center for the Study of Itch, Washington University School of Medicine, St. Louis, MO 63110

[4]Department of Quantitative and Systems Biology, University of California Merced, Merced, CA 95343

[5]Department of Pathology, University of California San Diego, La Jolla, CA 92093

[6]Department of Biomedical Sciences, Colorado State University, Fort Collins, CO 80523

[7]Department of Biological Science, Moberly Area Community College, Moberly, MO 65270

Abstract

The distance between nodes of Ranvier, referred to as internode length, positively correlates with axon diameter, and is optimized during development to ensure maximal neuronal conduction velocity. Following myelin loss, internode length is reestablished through remyelination. However, remyelination results in short internode lengths and reduced conduction rates. We analyzed the potential role of neurofilament phosphorylation in regulating internode length during remyelination and myelination. Following ethidium bromide induced demyelination, levels of neurofilament medium (NF-M) and heavy (NF-H) phosphorylation were unaffected. Preventing NF-M lysine-serine-proline (KSP) repeat phosphorylation increased internode length by 30% after remyelination. To further analyze the role of NF-M phosphorylation in regulating internode length, gene replacement was used to produce mice in which all KSP serine residues were replaced with glutamate to mimic constitutive phosphorylation. Mimicking constitutive KSP phosphorylation

[†]To whom correspondence should be addressed: Michael L. Garcia, Ph.D., Associate Professor, Division of Biological Sciences, University of Missouri, 209A LeFevre Hall, 1200 University Avenue, Columbia, MO 65211, Phone: 573-882-9712, GarciaML@missouri.edu.

[*]Authors contributed equally

Conflict of interest

The authors declare no conflicts of interest.

reduced internode length by 16% during myelination and motor nerve conduction velocity by ~27% without altering sensory nerve structure or function. Our results suggest that NF-M KSP phosphorylation is part of a cooperative mechanism between axons and Schwann cells that together determine internode length, and suggest motor and sensory axons utilize different mechanisms to establish internode length.

Keywords

Nerve injury; Remyelination; Reduced nerve conduction; Axon; Neurofilaments

Introduction

Postnatal development of peripheral nerves requires myelination and establishment of axonal diameter, which are required for rapid impulse transmission. Myelination includes formation of compact myelin and bidirectional elongation of myelinating Schwann cells along axons (Sherman and Brophy, 2005). While insights into the formation of compact myelin have been made, comparatively little is known about Schwann cell elongation. During development, there are two periods of Schwann cell elongation that establish internode length. The first period occurs during initial myelination from post-natal day 1 to approximately 14 days later, when myelination is complete (Webster, 1971). The initial period of elongation clusters ion channels (Dugandzija-Novakovic et al., 1995; Schafer et al., 2006; Vabnick et al., 1996) and establishes optimal internode length to maximize neuronal conduction velocity (Goldman and Albus, 1968; Hardy, 1971; Huxley and Stampfli, 1949). After initial establishment of internode length, Schwann cells continue to elongate during normal developmental growth to maintain optimal internode length and maximal conduction velocity (Bunge et al., 1989; Simpson et al., 2013; Vizoso, 1950).

A positive correlation between internode length and axon diameter was established over 140 years ago (Key and Retzius, 1875) such that larger diameter axons have longer internodes. Radial growth establishes axon diameter, and is dependent upon myelination (de Waegh et al., 1992). Myelination induces radial growth, so myelinated regions of an axon have larger diameters compared to unmyelinated regions of the same axon (nodes of Ranvier) (Yin et al., 1998). Increases in axonal diameter correlate with neurofilament (NF) number (Friede and Samorajski, 1970), which are the main cytoskeletal proteins of myelinated axons (Perrot et al., 2008). NFs are the intrinsic determinants of axonal diameter in myelinated axons (Eyer and Peterson, 1994; Ohara et al., 1993; Zhu et al., 1997). Furthermore, axonal neurofilaments are composed of three subunits namely NF-Light (NF-L), NF-Medium (NF-M), and NF-Heavy (NF-H), (Jones et al., 2016) of which NF-M determines axonal diameter (Elder et al., 1998; Garcia et al., 2003). Within myelinated axon regions, neurofilament heavy (NF-H) and medium (NF-M) become phosphorylated on C-terminal lysine-serine-proline (KSP) repeats (de Waegh et al., 1992; Julien and Mushynski, 1982) upon myelination (de Waegh et al., 1992; Yin et al., 1998). Moreover, NF composition varies with developmental stage (Shaw and Weber, 1982; Shen et al., 2010) and within central versus peripheral nervous systems (Yuan et al., 2006; Yuan et al., 2012). Thus, Schwann cell

elongation, radial axonal growth, and NF KSP phosphorylation occur in parallel during postnatal development.

After nerve injury, the positive correlation between internode length and axon diameter is lost (Hildebrand et al., 1985; Vizoso and Young, 1948). Remyelination results in uniformly short internodes (Hildebrand et al., 1987; Sanders and Whitteridge, 1946; Vizoso and Young, 1948) resulting in reduced conduction velocity (Court et al., 2004). Loss of myelin also reverts several axonal properties to a pre-myelin phenotype. Sodium channels, normally clustered within nodes of Ranvier become diffusely localized within the axonal plasma membrane after myelin loss (Boiko et al., 2001; Waxman et al., 2004). Demyelination results in re-expression of $Na_v1.2$ α subunit of voltage sensitive sodium channels (Craner et al., 2004; Schafer et al., 2006) and suppression of $Na_v1.6$ (Craner et al., 2004; Schafer et al., 2006), which is the predominant α subunit of myelinated peripheral nerves (Boiko et al., 2001; Schafer et al., 2006; Vabnick et al., 1996). However, one axonal property that does not revert to a pre-myelination phenotype is the phosphorylation status of NF proteins (Arroyo et al., 2004; Cole et al., 1994). In order for demyelinated axons to revert back and resemble developing axons before myelination (pre-myelination phenotype), both NF-M and NF-H would need to be dephosphorylated during demyelination. The significance of maintaining NF-M and NF-H phosphorylation during demyelination and after demyelination is unknown as the role of NF-M and NF-H KSP phosphorylation is unclear (Garcia et al., 2009).

In this study, we demonstrate that NF-M KSP phosphorylation is involved in regulating internode length during remyelination and myelination. Preventing NF-M KSP phosphorylation resulted in formation of longer internodes during remyelination. Mimicking constitutive NF-M KSP phosphorylation during normal myelination reduced internode length. These results provide the first mechanistic insights into reduced internode length that occurs with remyelination.

Materials and methods

Animals

Mice were housed in microisolator cages on a 12-h light/dark cycle, and were given food and water ad libitum. All procedures were in compliance with the University of Missouri and University of California San Diego Animal Care and Use Committees and with all local and federal laws governing the humane treatment of animals.

Nerve demyelination by Ethidium bromide injection

For demyelination experiments all mice used were 1 month old. Mice were placed under isoflurane anesthesia and the left sciatic nerve was exposed via an incision in the flank followed by separation of underlying musculature by blunt dissection. Utilizing pulled microcapillary needles 2 μL of 0.1% ethidium bromide in normal saline was injected into the middle third of the exposed sciatic nerve to induce demyelination. Uninjected controls received only a sham operation, but no injection. Saline injected animals received an injection of normal saline. The mice were allowed to recover and placed back in their cage. Successful injection of 2μL of 0.1% ethidium bromide into the sciatic nerve was confirmed

by a change in color of the nerve compared to the uninjected and saline injected controls. Seven days after injection, the animals injected with ethidium bromide displayed loss of function of the injected nerve, which is consistent with affected nerve function after an injury (Villalon et al., 2015). Furthermore, gross examination of the nerves at 7 days post-injected showed inflammation and discoloration of the ethidium bromide injected nerve, consistent with nerve demyelination (Supplementary Fig. 1). Sciatic nerves were collected for analysis at three different time points; maximal demyelination point, at 7 days post-injection; beginning of remyelination, 14 days post-injection; and complete remyelination point, 30 days post-injection (Bondan et al., 2009; Bondan and Monteiro Martins Mde, 2013; Riet-Correa et al., 2002). For detailed analysis of nerves after ethidium bromide injection, Swiss Webster mice were treated as described above. Seven days after injection, mice were killed by anesthetic overdose and decapitation and the sciatic nerve distal to the injection site removed into 2.5% glutaraldehyde before processing to resin blocks exactly as described elsewhere (Jolivalt et al. 2016) and viewing via a light microscope.

Detection and quantification of NF proteins by immunoblotting

Sciatic nerves (demyelination experiments) and L5 motor and sensory roots were harvested and snap frozen in liquid nitrogen or were homogenized immediately. Tissues were homogenized on ice in a buffer containing 50 mM Tris, pH 7.5, 0.5 mM EDTA, pH 8, and protease inhibitors were added according to manufacturer's instructions. (Complete Mini, Roche, Mannheim, Germany). An equal volume of lysis buffer containing 50 mM Tris, pH 7.5, 150 mM NaCl, 1% NP-40, 1% sodium deoxycholate, and 2% SDS was added. The homogenates were sonicated for 10 seconds 2X, then boiled for 10 minutes in a sand bath, and clarified by centrifugation at 16,000 g for 10 minutes. Protein concentration was determined using the Bio-Rad Protein Assay kit (Bio-Rad, Hercules, CA, USA). Protein extracts (5μg) were resolved on 7.5% SDS-polyacrylamide gels and transferred onto nitrocellulose membrane or stained with Coomassie-blue. NF-L, NF-M and NF-H were identified with polyclonal antibodies. Phosphorylated NF-H and NF-M were identified using a mouse monoclonal antibody that recognizes the protein in a phospho-dependent manner (SMI-31, Covance, Emeryville, CA, USA). Mouse and chicken primary antibodies were detected with donkey anti-mouse and goat anti-chicken secondary antibodies conjugated to IRdye-700X® infrared fluorophores (Rockland, Gilbertsville, PA, USA) respectively. Immunoreactive bands were visualized by infrared detection with an Odyssey image scanner (LICOR Biosciences, Lincoln, NE, USA). Quantification of immunoblots was performed by the relative optical density (ROD) method. Absolute intensities of the immunoreactive bands were obtained using Photoshop (Adobe Systems Inc.) and RODs were calculated in the following manner: [(NF protein mean intensity – background mean intensity)*(number of pixels)]/[(loading control band mean intensity - background intensity)*(number of pixels)]. As loading control the intensity of the smear on the coomassie stained gels was used as the stain intensity directly correlates with the amount of protein loaded in the gel. Optical densities of immunoreactive bands were calculated as follows: [(absolute intensity – background intensity)*(number of pixels)] Average optical densities for each genotype were calculated and compared to the wild type averages, which were arbitrarily set to a value of 1. All optical densities were analyzed for statistical significance by one-way ANOVA with

Holm-Sidak post hoc analysis for pair wise comparisons or by a Student's *t*-test (SigmaPlot, Systat Software).

Antibodies used

All antibodies used in this study are commercially available. No in-house produced antibodies were used. CPCA (Chicken Polyclonal Antibody)-NF-L, CPCA-NF-M, CPCA-NF-H, and CPCA-MBP antibodies were obtained from EnCor Biotechnology, Gainesville, FL, USA. CPCA-NF-M and CPCA-NF-H were both made against the KE region of NF-M and NF-H and detect both phosphorylated and unphosphorylated NFs (Harris et al., 1991; Shaw et al., 2005). SMI-31 anitbodies were obtained from BioLegend, San Diego, CA. SMI-31 is a monoclonal antibody that reacts with a phosphorylated epitope in phosphorylated neurofilament H and neurofilament M (Sternberger and Sternberger, 1983).

Teased fiber analysis

Mice were sacrificed and the sciatic nerve was exposed by blunt dissection (for demyelination experiments) and immediately extracted and processed as subsequently described. For L5 root teased fibers experiments, the mice were transcardially perfused with 0.1M PBS, pH 7.4 for no more than 5 minutes. The L5 root was dissected. The dorsal root was shortened relative to the ventral root for easy identification. In all cases the nerves or roots were submersion fixed in a 2.5M glutaraldehyde, 0.025M sodium cacodylate, pH 7.38 solution for 25 min at 4°C. The nerves or roots were then rinsed in 1X PBS for 5 minutes and transferred to a saturated solution of Sudan black in 70% ethanol and allowed to incubate for 1 hr at room temperature. The samples were then rinsed twice in 70% ethanol for 5 min and transferred to a 10% glycerin solution. Fifty to one hundred axon bundles were separated from the ventral root and the tibial branch of the sciatic nerve. The bundle was transferred to a super frost microscope slide containing a thin layer of a 10% aqueous solution of glycerin: BSA (1:1). Individual fibers were teased apart from the bundle and laid out on the glass slide. Fibers were then allowed to dry overnight on a 50°C hot plate. Digital photos of the fibers were taken using the AxioVision Digital Image Processing Software (Carl Zeiss MicroImaging). Internode lengths were measured using ImageJ (NIH). At least 200 internodes were measured from each tissue sample and at least 3 animals were used per genotype and treatment. An average of the internode lengths for each genotype was calculated and used for statistical analyses. The data was analyzed for variability using the SAS analytics software (SAS Institute Inc.). Possible influential outliers were calculated using a CooksD test and the data was analyzed for statistical significance using one-way nested ANOVA.

Site directed mutagenesis and construction of NF-M$^{S\rightarrow E}$ mice by gene replacement

A genomic clone isolated from mouse 129 SVJ library was used for construction of NF-M$^{S\rightarrow E}$ [a generous gift from J. P. Julien]. A ~1.1 kb *Acc*I/*Bcl*I fragment, containing all KSP repeats, was subcloned into pBluescript KS. Five oligonucleotides were designed to convert the phosphorylated KSP serine residues to glutamate (Supplementary Fig. 2A) using a PCR approach as previously described (Garcia et al., 2009). DNA sequence analysis confirmed the substitution of the 7 serine codons with glutamate codons without the introduction of additional sequence changes (data not shown). The modified NF-M fragment was recloned

back into the *nefm* gene. *Nefm* 5' UTR and 3' UTR regions were amplified from mouse 129SvEv genomic DNA to increase homology from 5 kb to a total of 8 kb. Diphtheria toxin alpha gene with poly adenylation (DT-ApA) clone was a generous gift from Y. Yanagawa and T. Yagi (Yanagawa et al., 1999). DT-ApA was introduced at the 3' end of the construct as a negative selection marker. Finally, the *nefl* 3' UTR and a PKG Neo cassette were cloned at the 3' end of *nefm* exon 3 (inserted at the *Sal*I and *Mlu*I sites, which were cloned into the *nefm* 3' UTR using a linker) (Supplementary Fig. 2B). The targeting construct was linearized with *Aat*II and electroporated into mouse 129SvEv ES cells (Millipore Corporation) by the MU Transgenic Core and selected with G418 at 250μg/ml (Joyner, 1994). Drug resistant colonies were amplified and screened by PCR at the 3' end and by Southern Blot at the 5' end. DNA sequence analysis (MU DNA Core) was used to ensure incorporation of the *nefm*$^{S\rightarrow E}$ exon 3. Four out of the 192 ES clones were identified to have undergone homologous recombination at both the 5' and 3' ends of the gene to produce the NF-M$^{S\rightarrow E}$ targeted allele. One of the positive ES cell clones was injected into mouse C57Bl6 blastocysts, and the MU Transgenic Core implanted blastocysts into the uteri of pseudo-pregnant surrogates. Six chimeric male mice were identified from the surrogates. Germ line transmission of the NF-M$^{S\rightarrow E}$ allele was confirmed by PCR amplification of genomic DNA purified from tail biopsies using Invitrogen Taq (Clonentech Laboratories, Inc., A Takara Bio Company, Madison, WI, USA) with the following primers: NF-M Exon 3 Forward-5'TGCAGAGGGAGAAGAAAGGAGAGGA3', NF-M 3'UTR Reverse Primer-5'AACTGGCGAATCCCTAGGTACAT3', NF-L 3'UTR Reverse Primer-5'GTTGACCTGATTGGGGAGAA3'. Mice of either sex were bred to homozygocity and wild type littermates were used as controls (Supplementary Fig. 2C).

Nerve conduction velocity measurements

Nerve conduction velocities were measured in the sciatic nerve, interossseus muscle system of 6-month-old as previously described (Jolivalt et al., 2009). In brief, mice were anesthetized with halothane (4% in O2 for induction, 2-3% for maintenance) with body temperature maintained at 37 °C by a heating lamp and thermal pad connected to a temperature regulator and a rectal thermistor probe. The sciatic nerve was stimulated with single supramaximal square wave pulses (4-8 V and 0.05 ms duration) via fine needle electrodes placed at the sciatic notch and Achilles tendon. Evoked early (M waves) and late (H waves) responses were recorded from the interossseus muscles of the ipsilateral foot via two fine needle electrodes and displayed on a digital storage oscilloscope. The distance between the two sites of stimulation was measured using calipers, and motor sciatic nerve conduction velocity was calculated using the M wave response and sensory sciatic nerve conduction velocity using the H wave response as previously described (Jolivalt et al., 2009). Measurements were made in triplicate from a minimum of six animals per genotype, and the median was used as the measure of velocity. Values were compared for overall statistical significance by a Student's *t*-test (InSat, GraphPad Software, la Jolla, CA, USA).

Tissue preparation for axon morphometry

Mice were euthanized and perfused transcardially with a fixative solution of 2.5% glutaraldehyde, 4% paraformaldehyde in 0.1 M cacodylate buffer, pH 7.2, and pos*t*-fixed overnight in the same buffer. Fifth lumbar nerve roots were dissected, treated with 2%

osmium tetroxide, washed, dehydrated, and embedded in Epon-Araldite resin. Thick sections (0.75 μm) for light microscopy were stained with ρ-phenylenediamine. Images of transverse sections of L5 motor axons were collected with a Zeiss Axio Imager A1 light microscope (Carl Zeiss MicroImaging GmbH, Jena, Germany) and analyzed in at least five mice per genotype and age group. Entire roots were imaged, imaging thresholds were selected individually, and the cross-sectional area of each axon was calculated and reported as a diameter of a circle of equivalent area using the AxioVision Digital Image Processing Software (Carl Zeiss MicroImaging). The total number of axons was analyzed for statistical significance by a two-way ANOVA (SigmaPlot, Systat Software, Inc.). Axonal diameters were grouped into 0.5 μm bins. Diameter distributions for 2-month-old motor axons were analyzed for overall statistical significance by a Mann-Whitney *U* test. Diameter distributions for 6-month-old motor and 2 and 6-month-old sensory axons were analyzed for statistical significance by a two-way ANOVA. G-ratios were calculated by measuring the axonal diameter and fiber diameter of individual axons for at least 10% of all axons per root (~ 100 axons for motor and ~250 axons for sensory) using AxioVision Digital Image Processing Software (Carl Zeiss Micro imaging). G-ratios were analyzed for statistical significance by a Student's *t*-test (SigmaPlot, Systat Software, Inc.).

Balance beam

Mice were trained 5 days to walk on three progressively smaller circular wooden beams (5, 2.5 and 1cm diameter) 120 cm in length, suspended 50 cm from a bedding surface. During training, mice walked on each of the three beams for 3 minutes with at least 20 minutes of rest. After training, experiments were performed on the smallest beam, which was marked in 5 cm increments. Mice walking on the beam were recorded using a digital camera for three trials per day for three consecutive days (9 total trials) with at least 20 minutes of rest between trials. Trials were recorded from two camera angles, parallel to the beam (6 trials) and perpendicular to the beam (3 trials). The number of falls, number of foot slips, total time walking, and the latency to fall within the 3-minute trials were scored from all 9 trials recorded. A fall was considered any event when the mouse fell off the beam, hanging under the beam was not considered a fall. Foot slips were events when the hind limbs of the mouse slipped off the surface of the beam. The total amount of time spent walking was measured from the beginning of a walking event to the end of that walking event. The total time walking per trial was calculated by adding the time of all individual walking events within a trial and it was used to normalize the number of falls and foot slips. Falling latency was calculated by measuring the time the mouse spent walking before each fall, therefore only mice that fell were included in this measurement. Average distance walked was calculated from the three perpendicular angle videos by using the 5 cm increment marks. To calculate the average walking speed, the time spent walking in the three perpendicular angle videos was also measured and together with the average distance walked was used to calculate the average velocity. The reported average time walked was also measured only from the three perpendicular angle videos. Averages of all observations were calculated for each genotype and analyzed for statistical significance by a Student's *t*-test.

Thermal algesia response latency

Latency response to noxious heat stimulus was measured as previously described (Calcutt, 2004). In brief, mice were placed on the warmed glass top surface of the testing apparatus and allowed to acclimate for 30 min. A mobile heating source was placed under the center of the hind paws and turned on. Turning on the heating source activated a timer and the heating source that locally heated the glass surface. When the animal responded to the stimulus by withdrawing its paw, movement sensors stopped the timer and the heating source. The time to response was recorded. Four measurements were taken for each paw with at least 5 min of rest between measurements. Both hind paws were tested and the average response time of both paws was used to calculate an average response for each mouse. Average response time across genotypes was analyzed for statistical significance by a Student's *t*-test.

Tactile algesia response threshold

Threshold response to tactile algesia was measured with a Dynamic Plantar Aesthesiometer (DPA) model # 37450 (Ugo Basile, Italy). Mice were set on a wire-mesh platform and allowed to habituate for at least 15 min. After habituation, the DPA monitored paw withdrawal thresholds of the hind and front paws. A metal filament was pushed against the hind and front paws with an ascending linear force (10 g/s and 2 g/s, respectively) until a strong, immediate withdrawal occurred. Measurements were taken in triplicate and averages were reported as paw withdrawal thresholds in grams. Averages for each paw were analyzed for statistical significance by a Student's *t*-test.

Results

Neurofilament heavy and medium subunits remained phosphorylated through remyelination

Internode length was reduced following remyelination (Hildebrand et al., 1987; Sanders and Whitteridge, 1946; Vizoso and Young, 1948). The observed reductions in internode length occurred in wild type tissue, which suggested that Schwann cells had the potential to re-establish wild type internode lengths following remyelination. Therefore, we hypothesized, that much like myelin thickness, axons might contribute to establishing internode length and that this could be altered during remyelination resulting in reduced internode length. As an initial approach, we used ethidium bromide (EtBr) injection as an established model for inducing demyelination in the sciatic nerve (Bondan et al., 2009. EtBr injections into sciatic nerves of 1-month-old wild type mice induced demyelination in an ~7mm long region along the injected nerve (Supplementary Figs. 1B and 3). Myelin loss compromised limb abduction and digit spreading in the tail suspension test (Supplementary Fig. 1A). Remyelination in EtBr injected sciatic nerves resulted in a 75% reduction in internode length at 30 days post injection (Supplementary Fig. 4). We analyzed NF protein and phosphorylation levels at 7, 14 and 30 days post-EtBr injections in 1-month-old mice. Sciatic nerve protein homogenates were resolved on 4% - 12% gradient SDS-PAGE gels. Myelin basic protein (MBP) levels were analyzed as a measure of myelination in uninjected controls (C), saline injected (S) and EtBr injected (I) sciatic nerves (Fig. 1A and 1B). No differences were apparent between C and S controls (Fig. 1A). Since no differences were found between C and S controls only comparisons between C nerves and I nerves are shown

for simplification. We utilized coomassie stained gels, which were run simultaneously, and ponceau S stained membranes, after overnight transfer, to ensure equal protein loading and equal protein transfer as our method for normalizing protein levels as previously described (Barry et al., 2012; Garcia et al., 2003; Garcia et al., 2009). Immunoblotts followed by relative optical density (ROD) analysis revealed reduced MBP levels beginning at day 7 and continuing throughout the time course ($p < 0.001$ at 7 and 14 days) with MBP levels beginning to recover by day 30 ($p = 0.005$) (Fig. 1B). Immunoblot and ROD analysis of neurofilament levels suggested an early decrease in all subunits ($p < 0.001$ for NF-L, $p = 0.015$ for NF-M, and $p = 0.004$ for NF-H) (Fig. 1C, 1D and 1F). Neurofilament light (NF-L) ($p < 0.001$) and medium (NF-M) ($p < 0.043$) remained reduced 14 days post-injection while neurofilament heavy (NF-H) recovered to pre-injection levels. By 30 days, NF-L and NF-M levels recovered to pre-injection levels, and NF-H levels were once again decreased ($p = 0.008$). Analysis of NF-H and NF-M phosphorylation levels suggested that the phosphorylation status of both subunits was unaltered during remyelination ($p > 0.05$) (Fig. 1E and 1G).

Preventing NF-M KSP repeat phosphorylation increased internode length following remyelination

Internode length positively correlates with axonal diameter (Key and Retzius, 1875). Several lines of genetically modified mice have identified NF-M as the critical subunit (Elder et al., 1998; Rao et al., 1998; Zhu et al., 1997) and NF-M C-terminus (Garcia et al., 2003) as the critical subdomain for establishing axon diameter. While the precise mechanism remains unclear, increasing the length of NF-M C-terminus resulted in increased axon diameter (Barry et al., 2012) independent of NF-M lysine-serine-proline (KSP) repeat phosphorylation (Garcia et al., 2009). We, therefore, focused our analysis on NF-M for the remainder of the study. NF-M phosphorylation occurs upon formation of compact myelin (de Waegh et al., 1992; Yin et al., 1998). Thus, Schwann cell elongation during myelination occurs when NF-M KSP repeats are not fully phosphorylated (de Waegh et al., 1992; Yin et al., 1998). To determine if NF-M KSP phosphorylation could influence internode development, we analyzed internode length following remyelination in a mouse model in which NF-M C-terminus cannot be phosphorylated due to the absence of this domain including the KSP sites (referred to as NF-$M^{\Delta T\ ail}$) (Garcia et al., 2003; Rao et al., 2003). Axons were teased from sciatic nerve of uninjected wild type and NF-$M^{\Delta T\ ail}$ mice (Fig. 2A) at 30 days post-injection of EtBr (Fig. 2B). Remyelination resulted in reduced internode length from both wild type ($p < 0.001$) and NF-$M^{\Delta T\ ail}$ ($p < 0.001$) mice relative to their uninjected controls. However, remyelination in NF-$M^{\Delta T\ ail}$ mice resulted in internode lengths that were significantly ($p = 0.039$) longer (30%) than those of remyelinated wild type nerves (Fig. 2C). Analysis of number of internodes within a 1 cm axonal segment showed that after remyelination both wild type ($p < 0.001$) and NF-$M^{\Delta T\ ail}$ ($p < 0.001$) nerves required significantly more internodes/cm relative to uninjured controls (Fig. 2D). Supportive of longer internodes NF-$M^{\Delta T\ ail}$ remyelinated nerves required ~20% ($p = 0.003$) fewer internodes/cm than wild type remyelinated nerves (~ 44 internodes/cm vs. 54 internodes/cm, respectively) (Fig. 2D). Taken together these data suggest that preventing NF-M KSP phosphorylation during remyelination increased internode lengths. However, we cannot rule out potential roles for other regions of the NF-M C-terminus, as NF-$M^{\Delta T\ ail}$ had

426 amino acids deleted from the C-terminus. Therefore, we generated and analyzed a novel line of NF-M mice in which all 7 serine residues of the C-terminal KSP repeats were mutated to glutamate (S→E) to mimic the charge associated with phosphorylation (Supplementary Fig. 2).

Expressing NF-M$^{S\rightarrow E}$ did not alter the electrophoretic mobility of NF-M or neurofilament subunit stoichiometry in sciatic nerve

Analysis of phospho-KSP-incompetent NF-M (referred to as NF-M$^{S\rightarrow A}$) mice revealed that preventing phosphorylation of NF-M KSP repeats increased the mobility of NF-M$^{S\rightarrow A}$ relative to wild type NF-M (Garcia et al., 2009). Upon SDS-PAGE fractionation, coomassie blue staining revealed that NF-M$^{S\rightarrow E}$ migrated at the same apparent molecular weight as wild type NF-M in tissue take from mice at 2 (Fig. 3A) and 6 months (Fig. 3D) of age. Immunoblotting with an antibody specific to the KE region (Harris et al., 1991) of NF-M C-terminus confirmed the identical electrophoretic mobilities of the wild type and NF-M$^{S\rightarrow E}$ proteins. ROD analysis of immunoblotting with subunit specific antibodies suggested similar levels of all neurofilament subunit proteins at 2 (Fig. 3B and 3C) and 6 months (Fig. 3E and 3F). No statistical differences were found in subunit expression at either time point following statistical analysis of RODs by one-way ANOVA followed by a Holm-Sidak *post hoc* analysis for pair wise comparisons.

Expressing NF-M$^{S\rightarrow E}$ increased NF-H phosphorylation in young mice but not in older mice

Preventing NF-M phosphorylation by C-terminal truncation (Garcia et al., 2003) or replacing KSP serine residues with alanines (Garcia et al., 2009) resulted in a compensatory increase in NF-H phosphorylation. To determine if mimicking constitutive phosphorylation of NF-M alters phosphorylation status of NF-H, a monoclonal antibody that detected phosphorylated NF epitopes was used to measure NF phosphorylation (Fig. 3G and 3I). SMI-31 reacted with phosphorylated NF-H at 2 (Fig. 3G) and 6 months (Fig. 3I) of age. At 2 months, ROD analysis suggested a significant ($p < 0.05$) increase in phosphorylation levels of NF-H in NF-M$^{S\rightarrow E/S\rightarrow E}$ mice compared to wild type (Fig. 3H). However, by 6 months, NF-H phosphorylation levels were similar in NF-M$^{S\rightarrow E/S\rightarrow E}$ and NF-M$^{wt/wt}$ (Fig. 3J). These data suggested that expressing NF-M$^{S\rightarrow E}$ did not result in overall compensatory increases in NF-H phosphorylation in older mice. Statistical analyses were done by one-way ANOVA followed by a Holm-Sidak *post hoc* analysis for pairwise comparisons.

Motor, but not sensory, nerve conduction velocity was reduced in NF-M$^{S\rightarrow E/S\rightarrow E}$ mice

We measured motor and sensory nerve conduction velocity (NCV) in 6-month-old NF-M$^{S\rightarrow E/S\rightarrow E}$ and NF-M$^{wt/wt}$ mice (Fig. 4A and 4B). Motor NCV was ~27% reduced in NF-M$^{S\rightarrow E/S\rightarrow E}$ mice relative to NF-M$^{wt/wt}$ littermate controls ($p = 0.0123$, student's T-test) (Fig. 4A). Sensory NCV was unaffected (Fig. 4B).

No alterations in axonal diameter of motor or sensory axons in mice expressing NF-M$^{S\rightarrow E}$

Three structural properties together determine the speed of neuronal conduction: axonal diameter, myelin thickness and internode length. To determine if mimicking phosphorylation of NF-M affected axon survival or growth, cross sections of the L5 motor (Fig. 5) and

sensory (Fig. 6) root were taken from 2 and m6-month-old NF-M$^{S\rightarrow E/S\rightarrow E}$ and NF-M$^{wt/wt}$ mice. There were no apparent differences in gross morphology (Fig. 5A and 6A) or axon number (Fig. 5B and 6B) at either time point for motor or sensory axons.

Cross-sectional areas were measured for all motor and sensory axons at both time points, and corresponding diameters were calculated. At 2 months, there was a 0.5μm increase in the peak axonal diameter of large diameter (> 4 μm) motor axons in NF-M$^{S\rightarrow E/S\rightarrow E}$ compared to NF-M$^{wt/wt}$ littermate controls (Fig. 5C). However, by 6 months, the diameters of all large diameter motor axons were indistinguishable between NF-M$^{S\rightarrow E/S\rightarrow E}$ and NF-M$^{wt/wt}$ mice (Fig. 5D). Small diameter motor axons (< 4μm) were similar at 2 months (Fig. 5C). However, at 6 months, the peak diameter for small diameter motor axons was 0.5 μm smaller in NF-M$^{S\rightarrow E/S\rightarrow E}$ compared to NF-M$^{wt/wt}$ (Fig. 5D). Axonal diameters of sensory axons were unaffected at 2 (Fig. 6C) or 6-months (Fig. 6D). Taken together these results suggested that alterations in axonal diameter were not the cause of reduced motor NCV in 6-month-old NF-M$^{S\rightarrow E/S\rightarrow E}$ mice.

Myelin thickness was unaltered in NF-M$^{S\rightarrow E/S\rightarrow E}$ mice

We next analyzed the ratio of axon diameter to fiber diameter (g-ratio) to determine if reduced motor NCV in NF-M$^{S\rightarrow E/S\rightarrow E}$ mice was due to alterations in myelin thickness (Fig. 7A). Ten percent of motor (~100) and sensory (~250) axons were randomly selected for g-ratio calculations. At both 2 and 6 months, g-ratios of small (Fig. 7B) and large (Fig. 7C) motor axons were similar between NF-M$^{S\rightarrow E/S\rightarrow E}$ and NF-M$^{wt/wt}$. NF-M$^{S\rightarrow E/S\rightarrow E}$ sensory axon g-ratios were also indistinguishable from NF-M$^{wt/wt}$ at 2 and 6 months (Fig. 7D). G-ratios were analyzed for statistical significance by Student's *t*-test, and no significant differences were found. These results suggested that decreased motor NCV of NF-M$^{S\rightarrow E/S\rightarrow E}$ mice also cannot be explained by alterations in myelin thickness.

Internode length of motor axons was reduced in NF-M$^{S\rightarrow E/S\rightarrow E}$ mice

Having eliminated alterations in axonal diameter and myelin thickness as potential explanations for reduced motor NCV, we analyzed the third structural property, internode length. Internode length was measured in teased fibers of the L5 motor from NF-M$^{S\rightarrow E/S\rightarrow E}$ and littermate control mice (Fig. 8A) and sensory (Fig. 8B) roots. Internode length was significantly reduced in motor (Fig. 8C) but not sensory (Fig. 8D) axons in 6-month-old NF-M$^{S\rightarrow E/S\rightarrow E}$ mice. Average internode length of motor axons was 927 ± 26 μm and 778 ± 45 μm for NF-M$^{wt/wt}$ and NF-M$^{S\rightarrow E/S\rightarrow E}$ mice, respectively (Fig. 8C). Average internode length of sensory axons was 831±34 μm for NF-M$^{wt/wt}$ and 851±16 for NF-M$^{S\rightarrow E/S\rightarrow E}$, respectively (Fig. 8D). Internode lengths were analyzed for statistical significance by Student's *t*-test. These results indicate that expressing NF-M$^{S\rightarrow E}$ resulted in a 16% decrease in motor axon internode length, which may contribute to reduced motor NCV and that these effects were specific to motor axons.

Expressing NF-M$^{S\rightarrow E/S\rightarrow E}$ reduced internode length early in myelination

During development, two phases of Schwann cell elongation establish and maintain internode length. The first phase occurs with normal developmental myelination (Webster, 1971), and the second phase occurs during growth (Jacobs, 1988). To determine which phase

was altered by expressing NF-M$^{S\rightarrow E/S\rightarrow E}$, we measured internode length over a time course (Fig. 9, see also Supplementary Fig. 5). Internode length was significantly reduced at 15 days (Fig. 9A), 1 month (Fig. 9B) and 6 months (Fig. 9C). Average internode lengths at 15 days were 475 ± 27μm and 382 ± 12μm for wild type and NF-M$^{S\rightarrow E/S\rightarrow E}$, respectively, which is approximately 20% reduced in NF-M$^{S\rightarrow E}$ mice. At 1 month, average internode lengths were approximately 16% reduced in NF-M$^{S\rightarrow E}$ mice (708 ± 25 μm and 598 ± 16 μm for wild type and NF-M$^{S\rightarrow E}$ mice, respectively), which is similar to the reduction measured at 6 months. These results suggested that NF-M$^{S\rightarrow E}$ reduced internode length during the early phase of Schwann cell elongation and that it was maintained through the subsequent phase.

Motor coordination was reduced in NF-M$^{S\rightarrow E/S\rightarrow E}$ mice

Decreased internode lengths and motor nerve conduction velocities are associated with deficits in motor coordination (Court et al., 2004; Wu et al., 2012). Our results show that at 2 months of age there are no alterations to axonal diameter, axon number or myelin thickness in either sensory or motor nerve, indicating that at this time point the only major alteration in NF-M$^{S\rightarrow E/S\rightarrow E}$ mice nerves was reduced internode length, which we predicted would reduce motor nerve conduction velocity. Motor coordination was, therefore, analyzed at 2 months on the balance beam, as this represents the earliest time point when we were confident axon structure, other than internode length was unaltered. Balance beam has been shown to provide a sensitive assessment of motor coordination in mice (Stanley et al., 2005). Relative to age matched controls NF-M$^{S\rightarrow E/S\rightarrow E}$ mice had a significantly higher rate of falls (Fig. 10A) ($p = 0.0142$) and foot slips (Fig. 10B) ($p = 0.045$). Moreover, NF-M$^{S\rightarrow E/S\rightarrow E}$ walked for a shorter period of time (not significant) (Fig. 10C) and a significantly shorter distance (Fig. 10D) ($p = 0.044$). However, the walking speed (Fig. 10E) and latency to fall (Fig. 10F) was similar in NF-M$^{S\rightarrow E/S\rightarrow E}$ and NF-M$^{wt/wt}$ controls. All measurements were analyzed for statistical significance by a Student's *t*-test. These results indicate that NF-M$^{S\rightarrow E/S\rightarrow E}$ mice have impaired motor coordination by 2 months of age.

Sensitivity to noxious heat stimulation and tactile stimulation were not altered in NF-M$^{S\rightarrow E/S\rightarrow E}$ mice

Internode length was significantly reduced in motor but not sensory axons. To determine if expressing NF-M$^{S\rightarrow E}$ altered sensory function, we measured response latency to thermal stimulus and response threshold to mechanical stimulus. Response to thermal stimulation was unaltered in NF-M$^{S\rightarrow E/S\rightarrow E}$ mice relative to age-matched controls (Fig. 10G). Moreover, the response threshold to mechanical stimulus was also unaltered in NF-M$^{S\rightarrow E/S\rightarrow E}$ mice (Fig. 10H). All measurements were analyzed for statistical significance by a Student's *t*-test. Taken together these results suggested that expressing NF-M$^{S\rightarrow E}$ did not alter sensory nerve function, which was consistent with our result of unaltered sensory nerve morphology.

Discussion

During developmental myelination, Lysine-Serine-Proline (KSP) repeats located within the C-termini of NF-M and NF-H become phosphorylated (de Waegh et al., 1992; Julien and

Mushynski, 1983; Yin et al., 1998). While it has been known that myelination influences NF phosphorylation (de Waegh et al., 1992; Hsieh et al., 1994), the role for NF KSP phosphorylation is unclear (Garcia et al., 2009). Our results suggest that myelin-dependent phosphorylation of NF-M KSP repeats is a key step in determining internode length, which was first observed over 140 years ago (Key and Retzius, 1875). Previous analyses have suggested that internode development occurs cell autonomously (Court et al., 2004; Wu et al., 2012). However, our results suggest that axons contribute to determining internode length. Therefore, we propose that internode length is established cooperatively between Schwann cells and axons. This is consistent with the cooperative mechanisms utilized to establish myelin thickness (Michailov et al., 2004; Taveggia et al., 2005). Loss of periaxin resulted in profound reductions in internode length (Court et al., 2004) suggesting a primary role in establishing internode length. These two results may not be contradictory. For example, it is possible that NF-M phosphorylation is part of an axonal mechanism that maintains internode length, which is established by periaxin mediated Schwann cell elongation. If this were the case, then the axonal mechanism would not be altered in periaxin deleted mice suggesting cell autonomy. Altering the spatial-temporal pattern of NF-M phosphorylation could result in premature initiation of mechanisms involved in maintaining internode length possibly resulting in reduced internode length.

Our results also provide a molecular basis for an empirical observation that was first made over 70 years ago (Vizoso and Young, 1948; Weiss and Hiscoe, 1948). The positive correlation between internode length and axon diameter is lost following remyelination since remyelinated internodes are uniformly short regardless of axon diameter (Gledhill et al., 1973; Vizoso and Young, 1948; Weiss and Hiscoe, 1948). Our data show that neurofilament phosphorylation is maintained after demyelination and throughout remyelination, which correlates with reduced internode length. Similarly, constitutive expression of the phosphomimetic NF-M$^{S\rightarrow E}$ results in reduced internode length following developmental myelination. Both scenarios present cases where the spatial-temporal dynamics of adding negative charge to NF-M C-terminal KSP repeats is independent of myelination. Our results demonstrate that altering these dynamics reduces internode length, which provides the first mechanistic insights into reduced internode length following remyelination. Although we do not propose NF-M phosphorylation is the sole regulator of internode length, our data clearly show that it is part of a mechanism that has the potential to regulate internode length.

NF-M C-terminus establishes motor axon diameter (Barry et al., 2012; Garcia et al., 2003). The prevailing hypothesis was that myelin dependent phosphorylation of NF-M KSP repeats established axon diameter (de Waegh et al., 1992; Garcia et al., 2003; Yin et al., 1998). However, preventing NF-M KSP phosphorylation (NF-M$^{S\rightarrow A}$ mice) had no effect on axon diameter (Garcia et al., 2009) making the role of NF-M phosphorylation unclear. Our results provide a clear function for NF-M KSP phosphorylation, establishing internode length. Moreover, our results shed light on the dependency of NF-M phosphorylation on myelination (de Waegh et al., 1992). Premature phosphorylation results in short internodes, which alters nerve function by reducing the rate of impulse propagation along an axon (Brill et al., 1977; Court et al., 2004). Linking NF-M KSP phosphorylation with myelination allows for development of optimal internode length with clear demarcation between myelinated internodes and developing nodes of Ranvier. Interestingly, this role for NF-M

phosphorylation is limited to motor axons. Expressing NF-M$^{S\rightarrow E}$ had no effect on sensory axon structure or function. In fact, altering NF proteins primarily affects motor axons (Rao et al., 2003; Rao et al., 2002) suggesting that motor and sensory axon development depend on different molecular mechanisms. Further analyses are required to investigate the disparity between motor and sensory axon development.

Lastly, our results provide a potential target for the development of therapies designed to enhance recovery from demyelinating diseases or from nerve injuries. Complete recovery from demyelination must include recovery of full- length internodes. Our results suggest that targeting neurofilament phosphorylation will enhance remyelination resulting in significantly longer internodes. Protein phosphatase 1 (Strack et al., 1997) and protein phosphatase 2A (Saito et al., 1995; Strack et al., 1997) have been co-purified with neurofilament proteins. Developing strategies for local delivery of small molecules that activate PP1 or PP2A could reduce neurofilament phosphorylation levels in demyelinated axonal segments allowing for longer internodes following remyelination.

Supplementary Material

Refer to Web version on PubMed Central for supplementary material.

Acknowledgments

This work was supported by Grants from National Science Foundation [0544602], University of Missouri Research Board and Missouri Spinal Cord Injuries Research Program to MLG and NIH award NS081082 to NAC. Salary support for MLG was provided by the University of Missouri—Columbia and the C. S. Bond Life Sciences Center. EVL was supported by the NIGMS Initiative for Maximizing Student Diversity (IMSD) grant to Dr. Mark Hannink [R25 GM056901]. DMB was supported by both the C. S. Bond Life Sciences Fellowship Program and the U.S. Department of Education, Graduate Assistance in Areas of National Need (GAANN) Program [P200A090233]. DSL was funded by a NIGMS Post-baccalaureate Research Education Program grant to Drs. John David and Chris Hardin [R25 GM064120]. Special thanks to Ms. Lada Micheas from the MU Social Sciences Statistical Center for helping us with some statistical analyses; Dr. Natalia Karasseva and the University of Missouri Transgenic Animal Core for the generation of gene-replacement chimeric mice; Brian Reigle for writing the scripts used in automated determination of numbers of axons in assigned groups for axonal diameter profiles and Victor Arballo and Jesus Macias Jr. for expert technical assistance.

References

Arroyo EJ, et al. Acute demyelination disrupts the molecular organization of peripheral nervous system nodes. J Comp Neurol. 2004; 479:424–34. [PubMed: 15514980]

Barry DM, et al. Expansion of neurofilament medium C terminus increases axonal diameter independent of increases in conduction velocity or myelin thickness. The Journal of neuroscience : the official journal of the Society for Neuroscience. 2012; 32:6209–19. [PubMed: 22553027]

Boiko T, et al. Compact myelin dictates the differential targeting of two sodium channel isoforms in the same axon. Neuron. 2001; 30:91–104. [PubMed: 11343647]

Bondan EF, et al. Ethidium bromide-induced demyelination in the sciatic nerve of diabetic rats. Arquivos de neuro-psiquiatria. 2009; 67:1066–1070. [PubMed: 20069221]

Bondan EF, Monteiro Martins Mde F. Cyclosporine improves remyelination in diabetic rats submitted to a gliotoxic demyelinating model in the brainstem. Microsc Res Tech. 2013; 76:714–22. [PubMed: 23613304]

Brill MH, et al. Conduction velocity and spike configuration in myelinated fibers: computed dependence on internode distance. Journal of Neurology, Neurosurgery & Psychiatry. 1977; 40:769–774.

Bunge RP, et al. Movements of the Schwann Cell Nucleus Implicate Progression of the Inner (Axon-related) Schwann Cell Process During Myelination. Journal of Cell Biology. 1989; 109:273–284. [PubMed: 2745552]

Calcutt NA. Modeling diabetic sensory neuropathy in rats. Methods Mol Med. 2004; 99:55–65. [PubMed: 15131329]

Cole JS, et al. Modulation of axon diameter and neurofilaments by hypomyelinating Schwann cells in transgenic mice. J Neurosci. 1994; 14:6956–66. [PubMed: 7965091]

Court FA, et al. Restricted growth of Schwann cells lacking Cajal bands slows conduction in myelinated nerves. Nature. 2004; 432:191–195.

Craner MJ, et al. Molecular changes in neurons in multiple sclerosis: altered axonal expression of Nav1.2 and Nav1.6 sodium channels and Na+/Ca2+ exchanger. Proc Natl Acad Sci U S A. 2004; 101:8168–73. [PubMed: 15148385]

de Waegh SM, et al. Local modulation of neurofilament phosphorylation, axonal caliber, and slow axonal transport by myelinating schwann cells. Cell. 1992; 68:451–463. [PubMed: 1371237]

Dugandzija-Novakovic S, et al. Clustering of Na+ channels and node of Ranvier formation in remyelinating axons. J Neurosci. 1995; 15:492–503. [PubMed: 7823157]

Elder GA, et al. Absence of the mid-sized neurofilament subunit decreases axonal calibers, levels of light neurofilament (NF-L), and neurofilament content. Journal of Cell Biology. 1998; 141:727–39. [PubMed: 9566972]

Eyer J, Peterson A. Neurofilament-deficient axons and perikaryal aggregates in viable transgenic mice expressing a neurofilament-beta- galactosidase fusion protein. Neuron. 1994; 12:389–405. [PubMed: 8110465]

Friede RL, Samorajski T. Axon caliber related to neurofilaments and microtubules in sciatic nerve fibers of rats and mice. The Anatomical record. 1970; 167:379–87. [PubMed: 5454590]

Garcia ML, et al. NF-M is an essential target for the myelin-directed “outside-in” signaling cascade that mediates radial axonal growth. The Journal of Cell Biology. 2003; 163:1011–20. [PubMed: 14662745]

Garcia ML, et al. Phosphorylation of highly conserved neurofilament medium KSP repeats is not required for myelin-dependent radial axonal growth. The Journal of neuroscience : the official journal of the Society for Neuroscience. 2009; 29:1277–84. [PubMed: 19193875]

Gledhill RF, et al. Pattern of remyelination in the CNS. Nature. 1973; 244:443–444. [PubMed: 4582500]

Goldman L, Albus JS. Computation of impulse conduction in myelinated fibers; theoretical basis of the velocity-diameter relation. Biophysical journal. 1968; 8:596–607. [PubMed: 5699798]

Hardy WL. Computed Dependence of Conduction Speed in Myelinated Axons on Geometric Parameters. Biophys Society Abstracts. 1971; 11:238a.

Harris J, et al. A molecular dissection of the carboxyterminal tails of the major neurofilament subunits NF-M and NF-H. Journal of neuroscience research. 1991; 30:47–62. [PubMed: 1724473]

Hildebrand C, et al. Myelin sheath remodelling in regenerated rat sciatic nerve. Brain Res. 1985; 358:163–70. [PubMed: 2416385]

Hildebrand C, et al. Nodal spacing along regenerated axons following a crush lesion of the developing rat sciatic nerve. Developmental Brain Research. 1987; 32:147–154.

Hsieh ST, et al. Regional modulation of neurofilament organization by myelination in normal axons. J Neurosci. 1994; 14:6392–401. [PubMed: 7965044]

Huxley AF, Stampfli R. Evidence for saltatory conduction in peripheral myelinated nerve fibers. J Physiol. 1949; 108:315–339.

Jacobs JM. On internodal length. J Anat. 1988; 157:153–162. [PubMed: 3198476]

Jacomy H, et al. Disruption of type IV intermediate filament network in mice lacking the neurofilament medium and heavy subunits. Journal of neurochemistry. 1999; 73:972–84. [PubMed: 10461886]

Jolivalt CG, et al. B vitamins alleviate indices of neuropathic pain in diabetic rats. European journal of pharmacology. 2009; 612:41–7. [PubMed: 19393643]

Jones MR, et al. Genetic Manipulation of Neurofilament Protein Phosphorylation. Methods Enzymol. 2016; 568:461–76. [PubMed: 26795480]

Joyner AL. Gene Targeting. A Practical Apporach. Die Nahrung. 1994; 38

Julien JP, Mushynski WE. Multiple phosphorylation sites in mammalian neurofilament polypeptides. J Biol Chem. 1982; 257:10467–70. [PubMed: 7202005]

Julien JP, Mushynski WE. The distribution of phosphorylation sites among identified proteolytic fragments of mammalian neurofilaments. J Biol Chem. 1983; 258:4019–25. [PubMed: 6339492]

Key, A., Retzius, G. Studien in der Anatomie des Nervensystems und des Bindegewebe. Vol. 2. Samson and Wallin; Stockholm: 1875. p. 228

Michailov GV, et al. Axonal neuregulin-1 regulates myelin sheath thickness. Science. 2004; 304:700–3. [PubMed: 15044753]

Ohara O, et al. Neurofilament deficiency in quail caused by nonsense mutation in neurofilament-L gene. J Cell Biology. 1993; 121:387–395.

Perrot R, et al. Review of the multiple aspects of neurofilament functions, and their possible contribution to neurodegeneration. Mol Neurobiol. 2008; 38:27–65. [PubMed: 18649148]

Rao MV, et al. The neurofilament middle molecular mass subunit carboxyl-terminal tail domains is essential for the radial growth and cytoskeletal architecture of axons but not for regulating neurofilament transport rate. The Journal of cell biology. 2003; 163:1021–31. [PubMed: 14662746]

Rao MV, et al. Gene replacement in mice reveals that the heavily phosphorylated tail of neurofilament heavy subunit does not affect axonal caliber or the transit of cargoes in slow axonal transport. The Journal of Cell Biology. 2002; 158:681–93. [PubMed: 12186852]

Rao MV, et al. Neurofilament-dependent radial growth of motor axons and axonal organization of neurofilaments does not require the neurofilament heavy subunit (NF-H) or its phosphorylation. The Journal of Cell Biology. 1998; 143:171–81. [PubMed: 9763429]

Riet-Correa G, et al. Ethidium bromide-induced demyelination of the sciatic nerve of adult Winstar rats. Braz J Med Biol Res. 2002; 35:99–104. [PubMed: 11743621]

Saito T, et al. Neurofilament-associated protein phosphatase 2A: its possible role in preserving neurofilaments in filamentous states. Biochemistry. 1995; 34:7376–84. [PubMed: 7779779]

Sanders FK, Whitteridge D. Conduction Velocity and Myelin Thickness in Regenerating Nerve Fibers. J Physiol. 1946; 105:162–174.

Schafer DP, et al. Early events in node of Ranvier formation during myelination and remyelination in the PNS. Neuron Glia Biol. 2006; 2:69–79. [PubMed: 16652168]

Shaw G, Weber K. Differential expression of neurofilament triplet proteins in brain development. Nature. 1982; 298:277–9. [PubMed: 7045694]

Shaw G, et al. Hyperphosphorylated neurofilament NF-H is a serum biomarker of axonal injury. Biochem Biophys Res Commun. 2005; 336:1268–77. [PubMed: 16176808]

Shen H, et al. Distal to proximal development of peripheral nerves requires the expression of neurofilament heavy. Neuroscience. 2010; 170:16–21. [PubMed: 20633607]

Sherman DL, Brophy PJ. Mechanisms of axon ensheathment and myelin growth. Nature reviews Neuroscience. 2005; 6:683–90. [PubMed: 16136172]

Simpson AH, et al. Effect of limb lengthening on internodal length and conduction velocity of peripheral nerve. The Journal of neuroscience : the official journal of the Society for Neuroscience. 2013; 33:4536–9. [PubMed: 23467369]

Stanley JL, et al. The mouse beam walking assay offers improved sensitivity over the mouse rotarod in determining motor coordination deficits induced by benzodiazepines. J Psychopharmacol. 2005; 19:221–7. [PubMed: 15888506]

Sternberger LA, Sternberger NH. Monoclonal antibodies distinguish phosphorylated and nonphosphorylated forms of neurofilaments in situ. Proc Natl Acad Sci U S A. 1983; 80:6126–30. [PubMed: 6577472]

Strack S, et al. Protein serine/threonine phosphatase 1 and 2A associate with and dephosphorylate neurofilaments. Brain Res Mol Brain Res. 1997; 49:15–28. [PubMed: 9387859]

Taveggia C, et al. Neuregulin-1 type III determines the ensheathment fate of axons. Neuron. 2005; 47:681–94. [PubMed: 16129398]

Tepavčević, V., Baron-Van Evercooren, A. Transplantation of Myelin Forming Cells. In: Squire, LR., editor. Encyclopedia of Neuroscience. Elsevier Ltd; Netherlands: 2009. p. 1141-1152.

Vabnick I, et al. The clustering of axonal sodium channels during development of the peripheral nervous system. J Neurosci. 1996; 16:4914–22. [PubMed: 8756423]

Villalon E, et al. Exacerbation of Charcot-Marie-Tooth type 2E neuropathy following traumatic nerve injury. Brain Res. 2015; 1627:143–53. [PubMed: 26423936]

Vizoso AD. The relationship between intenodal length and growth in human nerves. J Anat. 1950; 84:342–353. [PubMed: 14794550]

Vizoso AD, Young JZ. Internode length and fibre diameter in developing and regenerating nerves. J Anat. 1948; 82:191–195.

Waxman SG, et al. Na+ channel expression along axons in multiple sclerosis and its models. Trends Pharmacol Sci. 2004; 25:584–91. [PubMed: 15491781]

Webster H. The geometry of the peripheral myelin sheaths during their formation and growth in rat sciatic nerves. Journal of Cell Biology. 1971; 48:348–367. [PubMed: 4928020]

Weiss P, Hiscoe HB. Experiments on the mechanism of nerve growth. Journal of Experimental Zoology. 1948; 107:315–395. [PubMed: 18915618]

Wu LM, et al. Increasing internodal distance in myelinated nerves accelerates nerve conduction to a flat maximum. Current biology : CB. 2012; 22:1957–61. [PubMed: 23022068]

Yanagawa Y, et al. Enrichment and efficient screening of ES cells containing a targeted mutation: the use of DT-A gene with the polyadenylation signal as a negative selection maker. Transgenic Res. 1999; 8:215–21. [PubMed: 10478491]

Yin X, et al. Myelin-associated glycoprotein is a myelin signal that modulates the caliber of myelinated axons. Journal of Neuroscience. 1998; 18:1953–1962. [PubMed: 9482781]

Yuan A, et al. Alpha-internexin is structurally and functionally associated with the neurofilament triplet proteins in the mature CNS. The Journal of neuroscience : the official journal of the Society for Neuroscience. 2006; 26:10006–19. [PubMed: 17005864]

Yuan A, et al. Peripherin is a subunit of peripheral nerve neurofilaments: implications for differential vulnerability of CNS and peripheral nervous system axons. The Journal of neuroscience : the official journal of the Society for Neuroscience. 2012; 32:8501–8. [PubMed: 22723690]

Zhu Q, et al. Delayed maturation of regenerating myelinated axons in mouse lacking neurofilaments. Experimental Neurology. 1997:299–316.

Abbreviations

NF	neurofilament
NF-L	neurofilament light
NF-M	neurofilament medium
NF-H	Neurofilament heavy
KSP	Lysine-Serine-Proline
Na_v	Voltage gated sodium channel
EtBr	Ethidium bromide
MBP	Myelin basic protein
ROD	Relative optical density

Highlights

- Axonal NF-M remains phosphorylated after demyelination and through remyelination.
- NF-M phosphorylation is part of a cooperative mechanism that determines internode length.
- NF-M phosphorylation influences internode length establishment in motor but not in sensory axons.

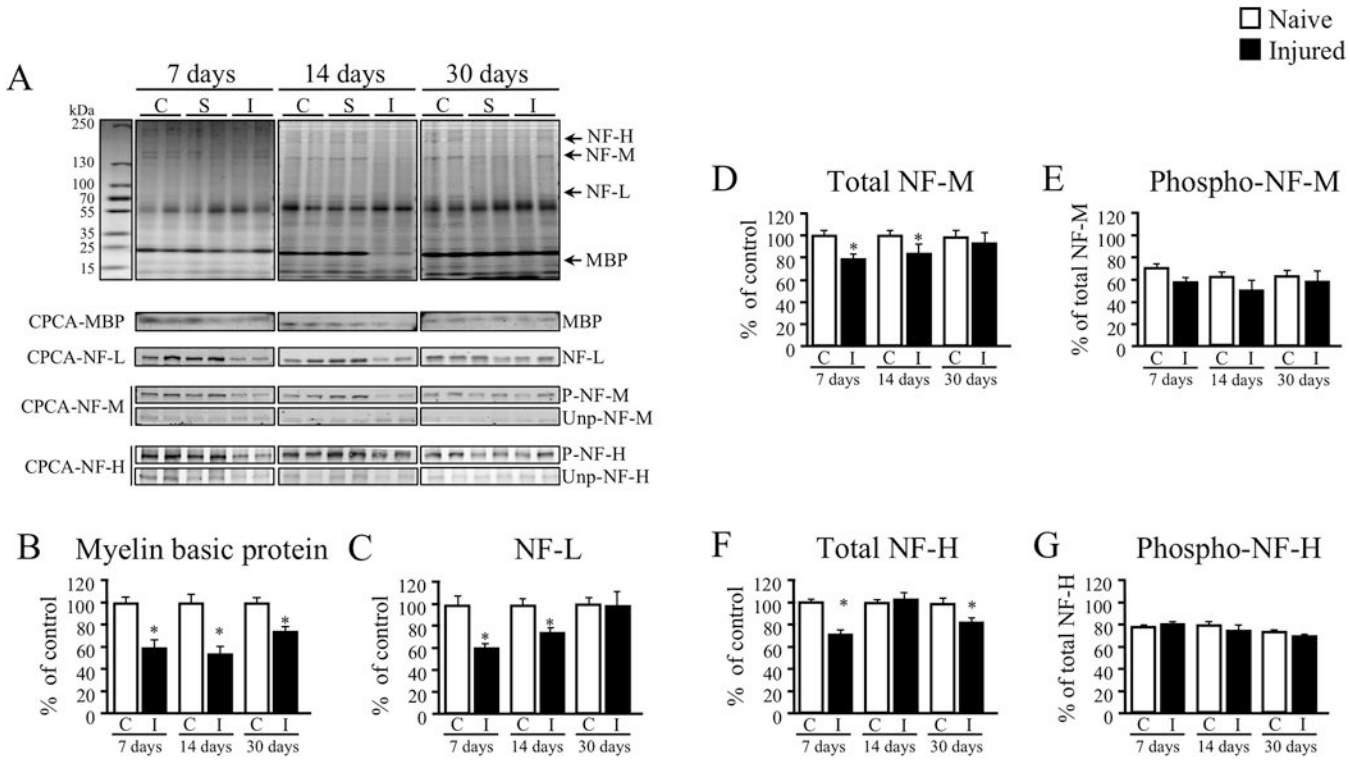

Fig. 1. Neurofilament phosphorylation levels were maintained during remyelination

(A) Sciatic nerve protein extract from 7, 14, and 30 days post ethidium bromide (EtBr) injections were resolved on 4% - 12% gradient SDS-PAGE gels and stained with Coomassie blue. Coomassie stained gels were used to verify equal protein loading and the intensity of the smear was used as loading control. RODs suggested decreases in myelin basic protein (MBP) at 7 and 14 days post-injection that slightly recovered by 30 days post-injection (B). Total NF-L (C) and NF-M (D) levels were decreased 7 and 14 days post-injection recovering to control levels by 30 days. Total NF-H was decreased 7 and 30 days post-injection (F). Phosphorylated NF-M (E) and NF-H (G) levels were not different at any time point. RODs were analyzed for statistical significance by a two-way ANOVA followed by Holm Sidak *post-hoc* test. Error bars = SEM. N = 5. C, uninjected control. S, saline injected control. I, ethidium bromide injected. P-NF-M/H = phosphorylated NF-M/H. Unp-NF-M/H = unphosphorylated NF-M/H

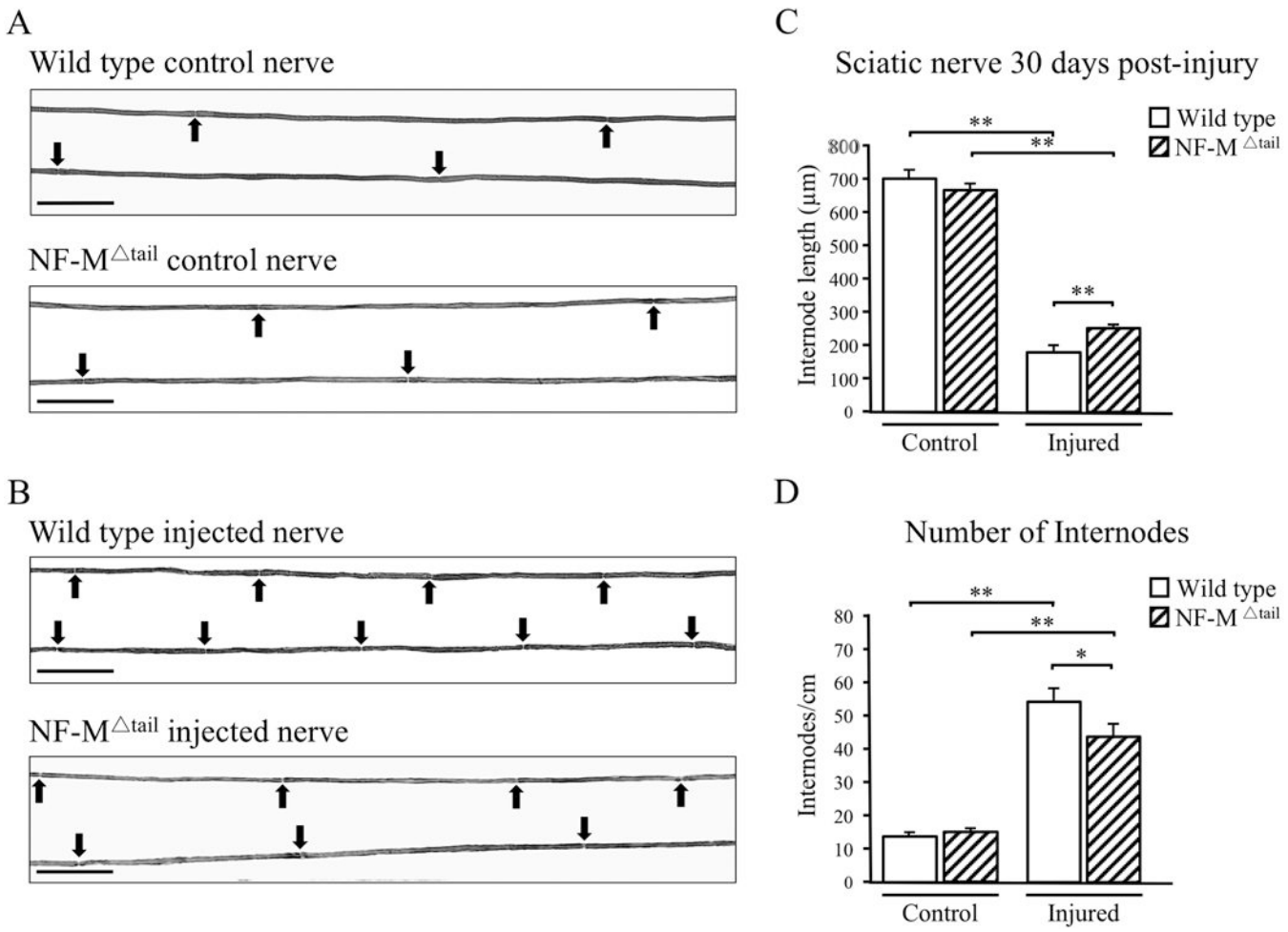

Fig. 2. Preventing NF-M KSP phosphorylation increased internode length after remyelination

(A) Thirty days post-injection revealed no apparent difference in internode length between uninjected wild type (top) and NF-M$^{\Delta T\ ail}$ controls (bottom). (B) Thirty days post-injection internode length was reduced in both wild type (top) and NF-M$^{\Delta T\ ail}$ mice (bottom) relative to uninjected controls. (C) Quantification of internode length revealed the expected decrease in internode length between control and injected nerves at 30 days post-injection. However, internode length was ~ 30% longer in NF-M$^{\Delta T\ ail}$ nerves. (D) The number of internodes required to myelinate a 1cm long axon segment was increased in both injected wild type and NF-M$^{\Delta T\ ail}$ nerves. Consistent with longer internode length injected NF-M$^{\Delta T\ ail}$ nerves required ~20% fewer internodes to myelinate the same axonal length. Averages per group were obtained and analyzed for statistical significance by a two-way ANOVA followed by a Holm Sidak *post-hoc* analysis. Error bars = SEM. N ≥ 4. Black arrow = node of Raniver. Scale bar = 100μm.

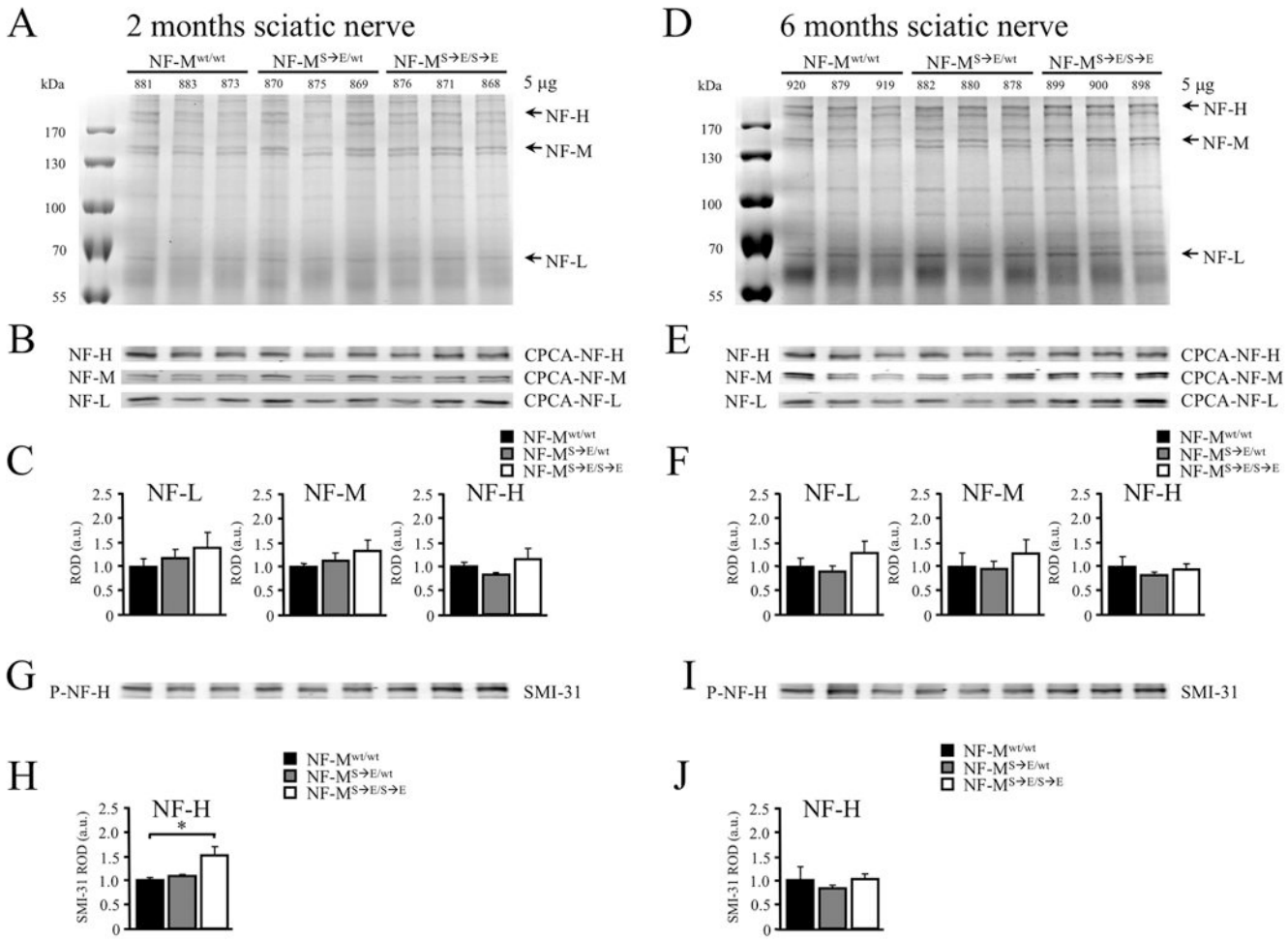

Fig. 3. Expressing NF-M$^{S\rightarrow E}$ reduced phosphorylation dependent detection of NF-M in young mice

(A and D) Sciatic nerve protein extract from 2 and 6-month-old NF-M$^{wt/wt}$, NF-M$^{wt/S\rightarrow E}$, and NF-M$^{S\rightarrow E/S\rightarrow E}$ mice were resolved on a 7.5% SDS-polyacrylamide gel and stained with Coomassie Blue. NF-M mobility was not affected by expression of NF-M$^{S\rightarrow E}$ in the sciatic nerve. (B and E) Sciatic nerve extracts from 2 and 6-month-old mice were immunoblotted with antibodies that recognize NF-L (CPCA-NF-L), NF-M (CPCA-NF-M), and NF-H (CPCA-NF-H). Immunoblotts confirmed that NF-M$^{S\rightarrow E}$ mobility was unaffected. (C and F) Relative optical densities (RODs) of immunoblotts suggested that neurofilament subunit stoichiometry was not altered in NF-M$^{S\rightarrow E/S\rightarrow E}$ or NF-M$^{S\rightarrow E/wt}$ mice relative to wild type. (G and I) Sciatic nerve extracts from 2 and 6 month-old mice were immunoblotted with an antibody that detects NF-H and NF-M in a phospho-dependent manner (SMI-31). (H and J) RODs suggested that the phospho-dependent antibody SMI-31 detected a significant increase in NF-H in NF-M$^{S\rightarrow E/S\rightarrow E}$ mice and a significant decrease in NF-M in NF-M$^{S\rightarrow E/wt}$ at 2 months compared to NF-M$^{wt/wt}$ mice (H). No alteration in NF-H or NF-M detection at 6 months was observed (J). ROD's were analyzed by one-way ANOVA. *, $p < 0.05$. Error bars = SEM. N= 3.

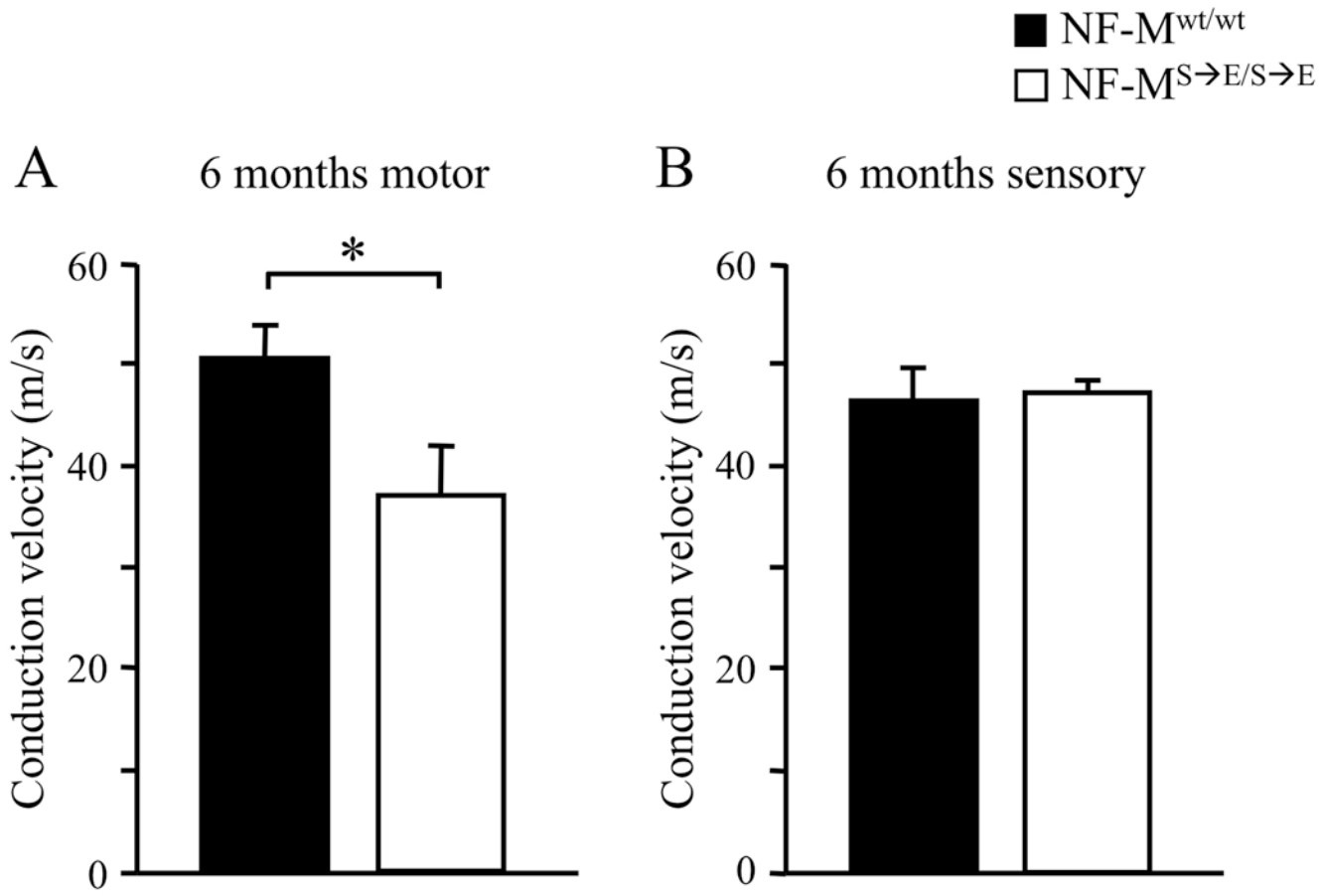

Fig. 4. Motor, but not sensory, nerve conduction velocity was significantly reduced in NF-M$^{S\rightarrow E}$ mice

Motor and sensory nerve conduction velocity (NCV) was measured from sciatic nerve in 6-month-old NF-M$^{wt/wt}$ and NF-M$^{S\rightarrow E/S\rightarrow E}$ mice. NCV analysis revealed a ~27% decrease in motor NCV in NF-M$^{S\rightarrow E/S\rightarrow E}$ mice (A). (B) Sensory NCV conduction velocity was indistinguishable between NF-M$^{S\rightarrow E/S\rightarrow E}$ and NF-M$^{wt/wt}$ controls. Nerve conduction velocities were analyzed by Student's *t*-test. *, $p < 0.05$. Error bars = SEM. N= 6.

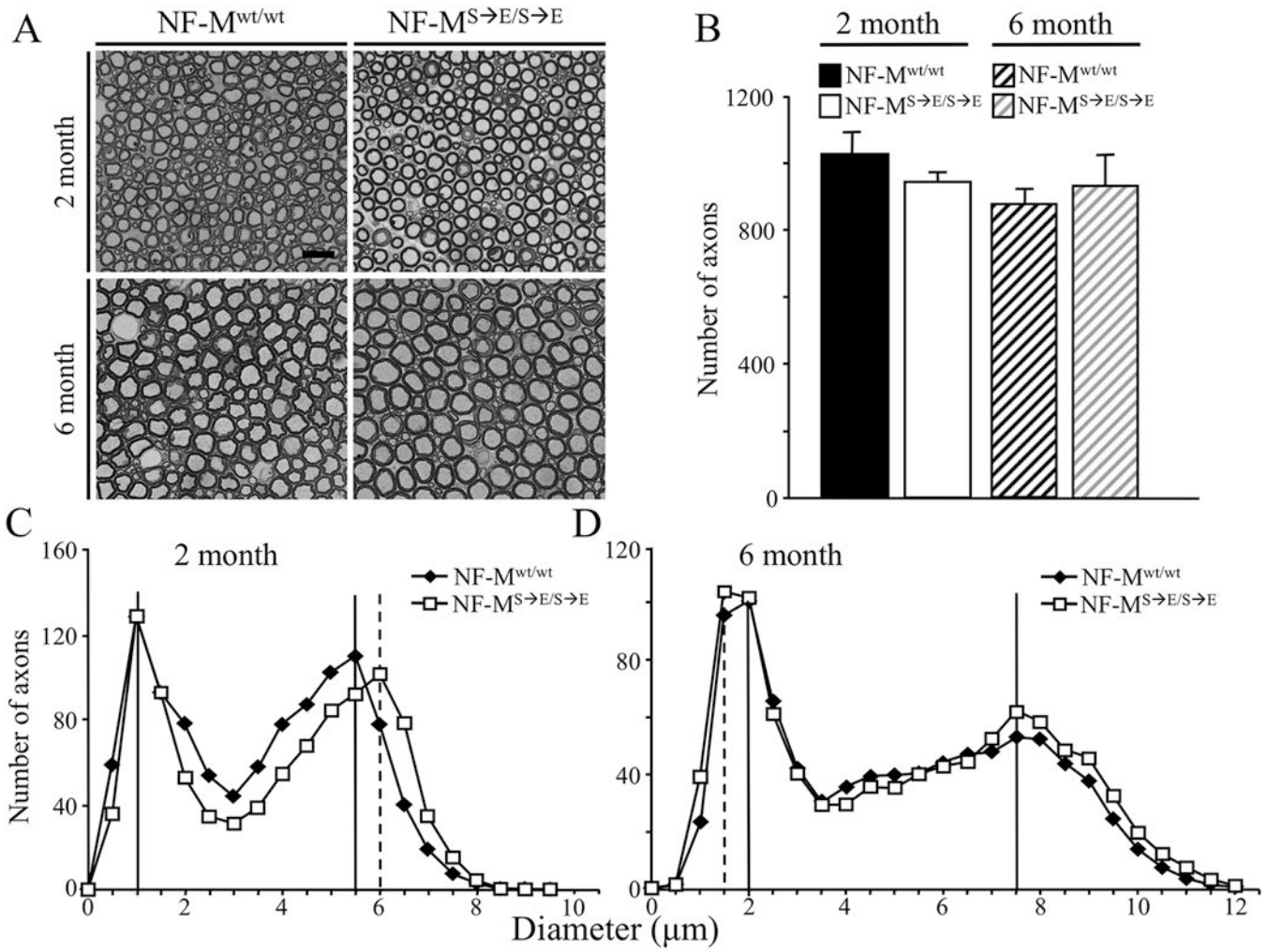

Fig. 5. Expressing NF-M$^{S\rightarrow E}$ did not alter motor axon diameter or survival

(A) Cross sections of the fifth lumbar motor (ventral) root (L5) from wild type and NF-M$^{S\rightarrow E/S\rightarrow E}$ mice at 2 and 6 months. Scale bar, 10 μm. (B) Motor axon number was unaltered at 2 and 6 months in wild type and NF-M$^{S\rightarrow E/S\rightarrow E}$ mice. (C and D) Axon diameter distribution from NF-M$^{wt/wt}$ and NF-M$^{S\rightarrow E/S\rightarrow E}$ mice at 2 and 6 months. Initially, NF-M$^{S\rightarrow E/S\rightarrow E}$ mice had a 0.5μm increase (not significant) in radial growth in large diameter motor axons (C). By 6 months, diameter distributions of large motor axons are indistinguishable between NF-M$^{S\rightarrow E/S\rightarrow E}$ and NF-M$^{wt/wt}$ mice (D). However, there was a 0.5μm (not significant) decrease in the diameter of small motor axons in NF-M$^{S\rightarrow E/S\rightarrow E}$ mice. Vertical lines in C and D identify peak diameters for small and large motor axons. N=6. Error bars = SEM. Axon counts were averaged from 5 animals per genotype per time point and analyzed for statistical significance by a two-way ANOVA.

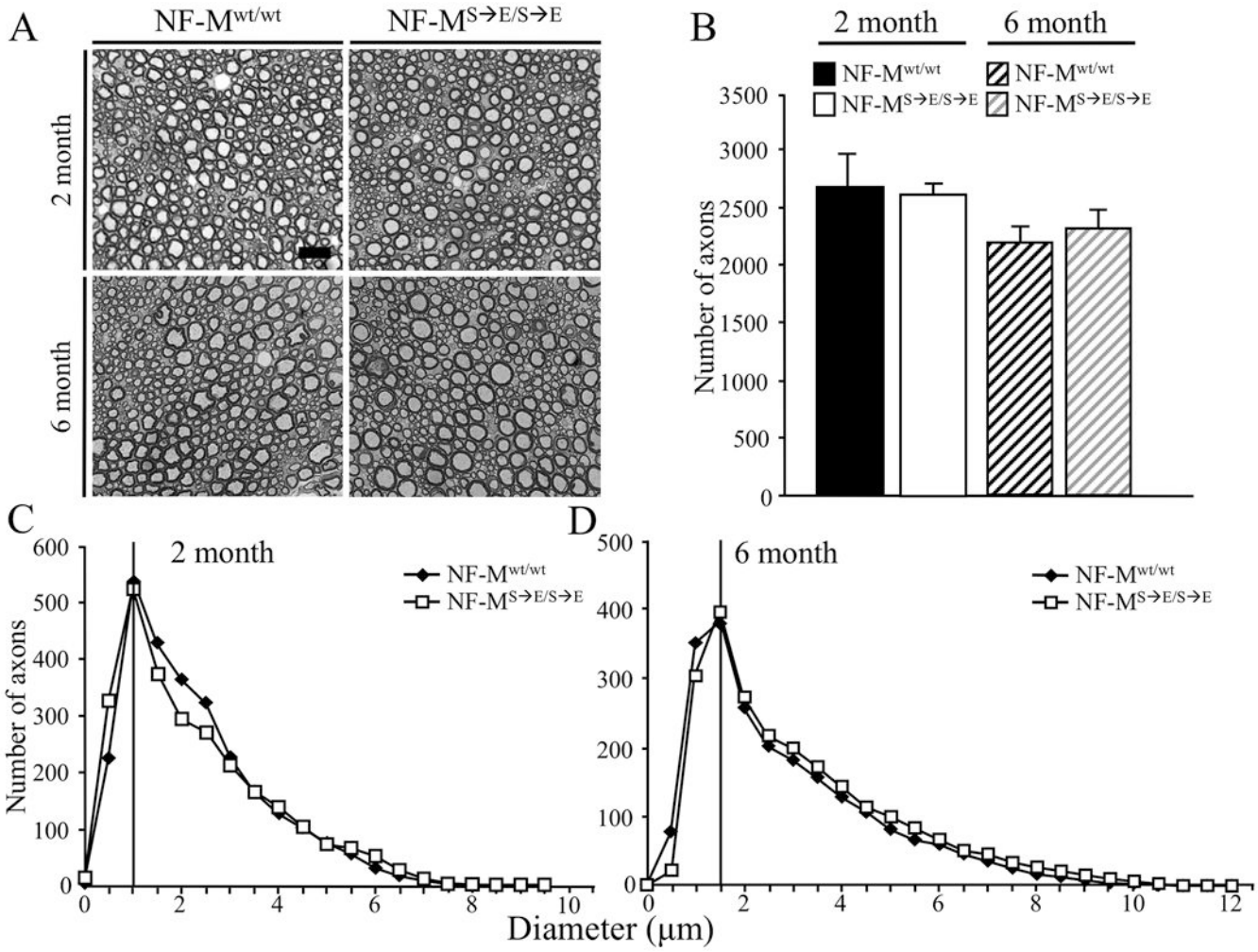

Fig. 6. Expressing NF-M$^{S\rightarrow E}$ did not affect sensory axons

(A) Cross-sections of the fifth lumbar sensory root from NF-M$^{wt/wt}$ and NF-M$^{S\rightarrow E/S\rightarrow E}$ mice at 2 and 6 months. Scale bar, 10 μm. (B) Sensory axon number was unaltered at 2 and 6 months in wild type and NF-M$^{S\rightarrow E/S\rightarrow E}$ mice. (C and D) Axon diameter distribution from NF-M$^{wt/wt}$ and NF-M$^{S\rightarrow E/S\rightarrow E}$ mice at 2 (C) and 6 (D) months. Peak diameters at both 2 (C) and 6 (D) were indistinguishable between NF-M$^{S\rightarrow E/S\rightarrow E}$ and NF-M$^{wt/wt}$. Vertical lines in C and C identify peak diameters for sensory axons. Error bars = SEM. Axon counts were averaged from 5 animals per genotype per time point and analyzed for statistical significance by a two-way ANOVA.

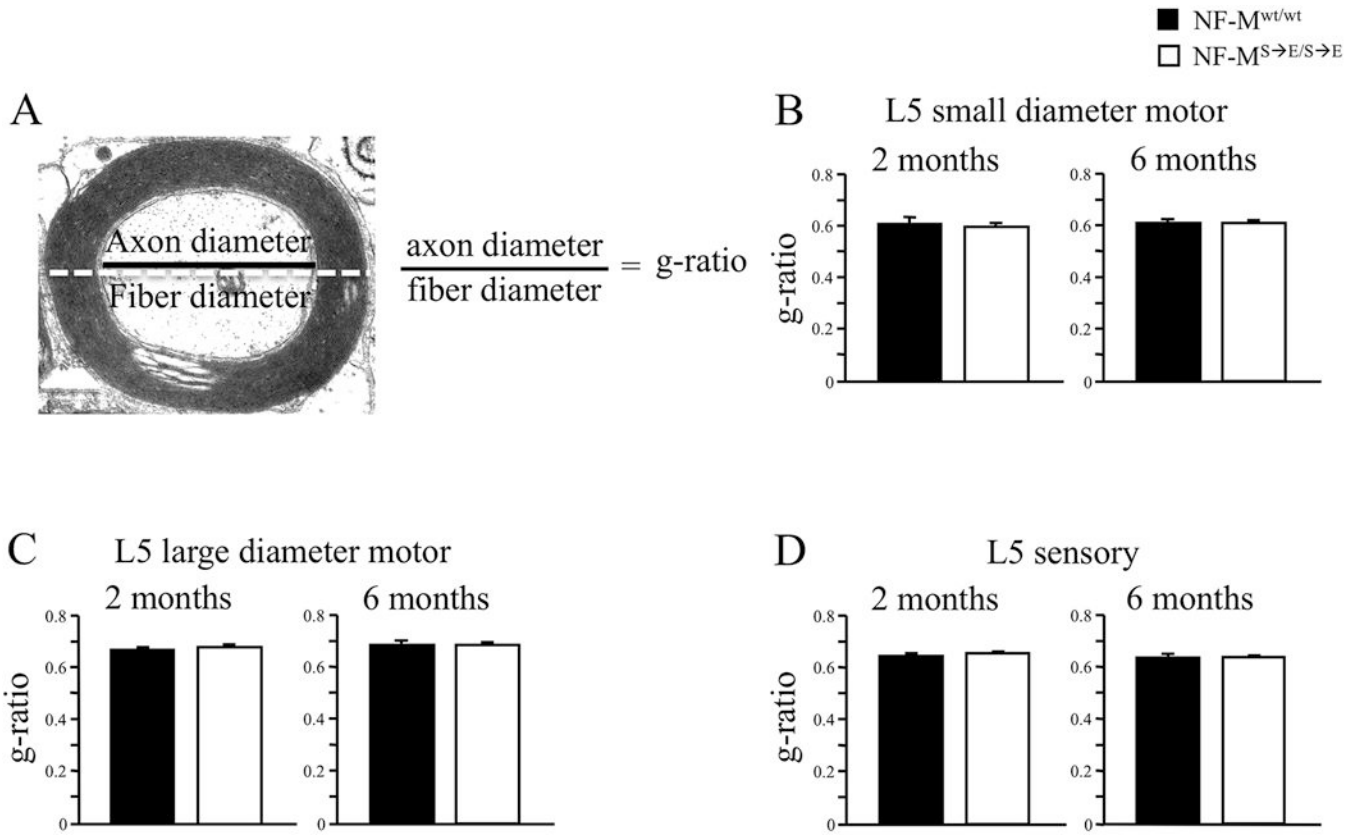

Fig. 7. Myelin thickness was not affected in NF-M$^{S\rightarrow E}$ mice

(A) Schematic of measurements used to calculate g-ratios (g-ratio: axon diameter/fiber diameter) from 10% of large motor, small motor axons and sensory. (B, C and D) Analysis of axon diameter and myelin thickness suggested that g-ratio was unaltered in small motor (C), large motor (D), or sensory (E) L5 root axons. Results were analyzed for statistical significance with a Student's *t*-test. Error bars = SEM. N = 12.

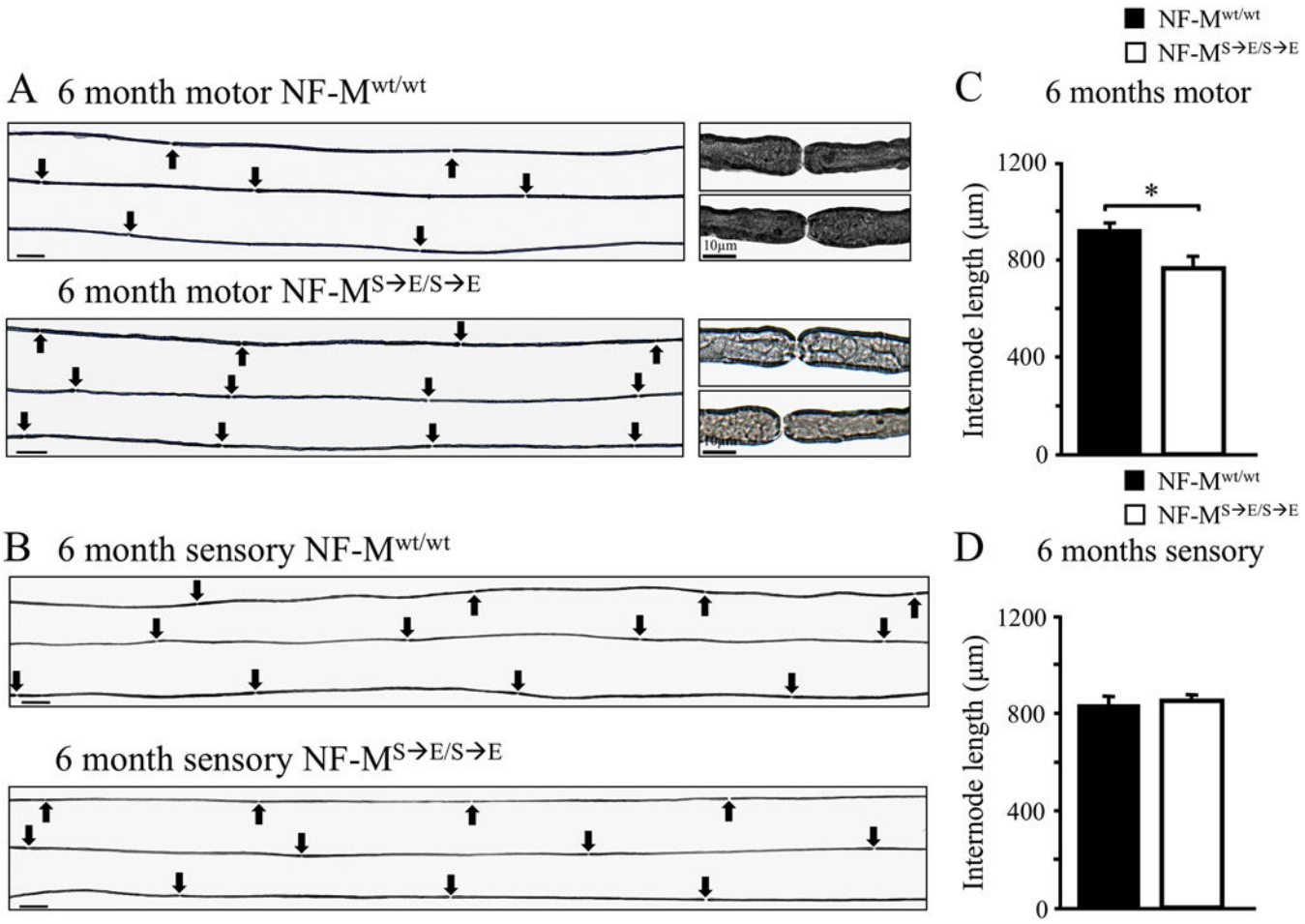

Fig. 8. Internode length was decreased in L5 motor axons in NF-M$^{S\rightarrow E/S\rightarrow E}$ mice

(A and B) Individual axons were teased from the L5 motor (A) and sensory (B) roots from 6-month-old NF-M$^{wt/wt}$ and NF-M$^{S\rightarrow E/S\rightarrow E}$ mice. Arrowheads identified the location of nodes of Ranvier. (A and B) Gross morphology of the nodes of Ranvier in L5 motor (A) and sensory (B) axons does not appear to be altered in NF-M$^{S\rightarrow E/S\rightarrow E}$ mice compared to wild type controls. (C and D) ~ 5 internodes per axon from ~ 100 axons were analyzed for motor and ~ 4 internodes per axon from ~ 40 axons for sensory nerves were measured and analyzed from NF-M$^{S\rightarrow E/S\rightarrow E}$ and NF-M$^{wt/wt}$ mice. Analysis of teased fibers suggested that average internode length was significantly reduced in motor (C) but not sensory (D) axons of NF-M$^{S\rightarrow E/S\rightarrow E}$ mice. Internode lengths were averaged and analyzed for statistical significance using a one-way nested ANOVA. *, $p < 0.05$. Error bars = SEM. N = 3.

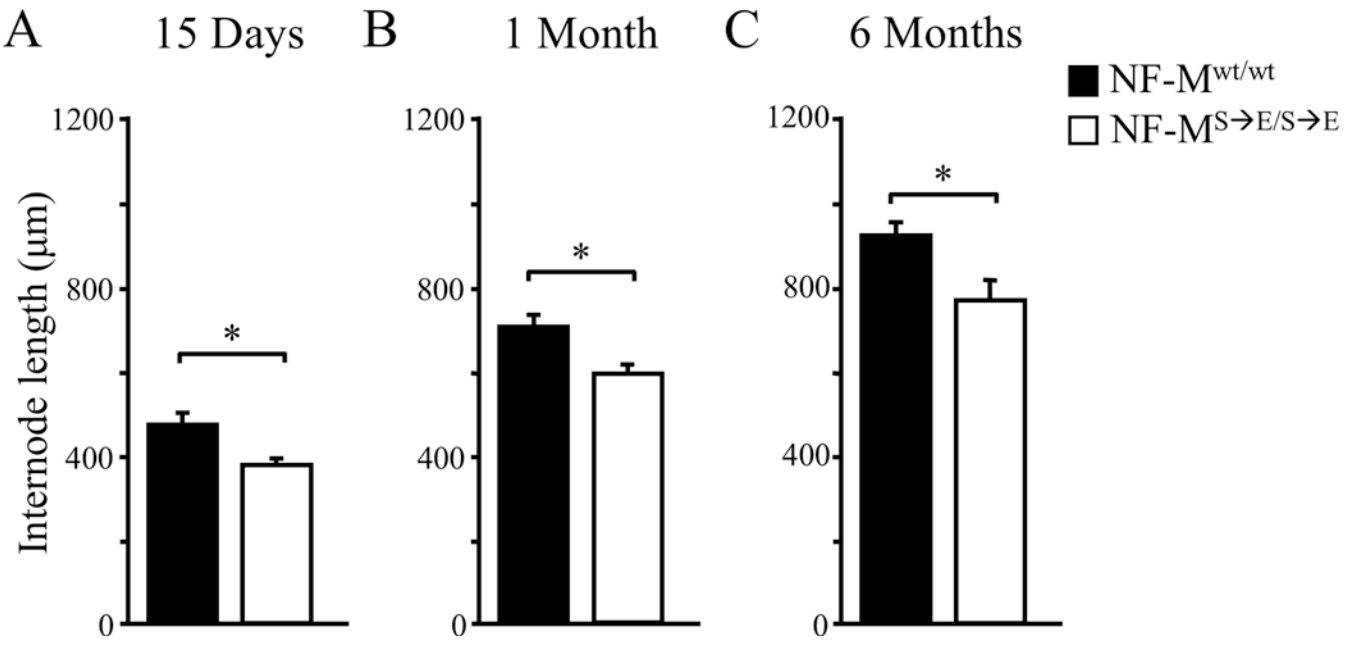

Fig. 9. Expressing NF-M$^{S\rightarrow E}$ altered both phases of Schwan cell elongation

(A, B and C) Time course analysis of L5 motor axon internode length in NF-M$^{S\rightarrow E/S\rightarrow E}$ mice at 15 days, 1 month and 6 months post birth. (A, B) ~ 200 internodes from varying number of L5 motor axons were measured from each animal at 15 days and 1-month postnatal. (C) L5 motor root teased fibers at 6-months as described in Fig. legend 9. Analysis of teased fibers suggested that average internode length was reduced at 15 days (A), 1 month (B) and 6 months (C). Average internode length was reduced by ~20%, ~16% and ~16% at 15 days, 1 month and 6 months, respectively. Internode lengths were averaged and analyzed for statistical significance using one-way nested ANOVA. *, $p < 0.05$. Error bars = SEM. N = 3 and 4 for NF-M$^{wt/wt}$ and NF-M$^{S\rightarrow E/S\rightarrow E}$ at 15 days, respectively. N = 5 for both NF-M$^{wt/wt}$ and NF-M$^{S\rightarrow E/S\rightarrow E}$ at 1 month.

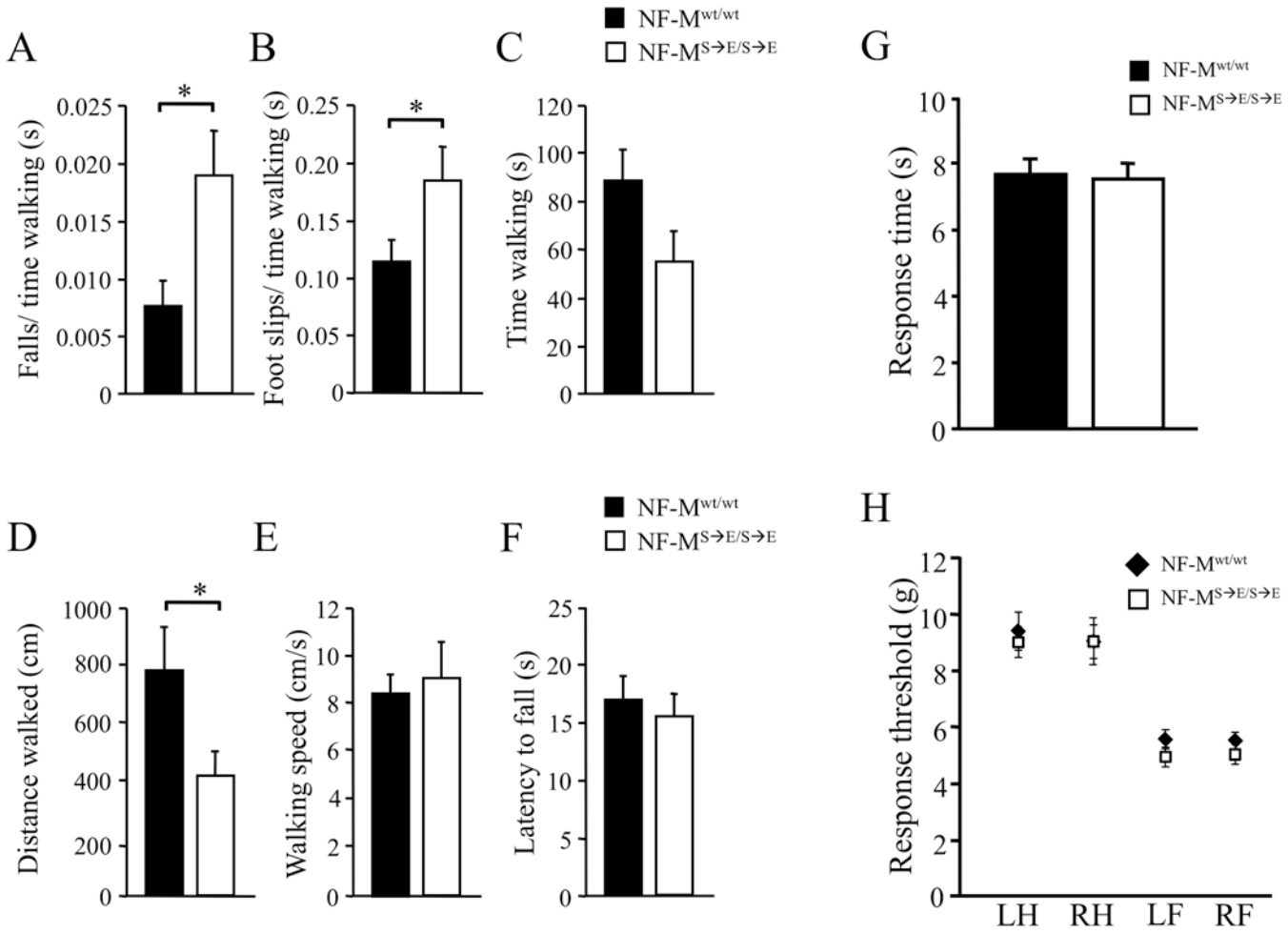

Fig. 10. Motor coordination, but not sensory nerve function was reduced in NF-M$^{S\rightarrow E/S\rightarrow E}$ mice

(A, B, C, D, E and F) Analysis of mouse performance on a balance beam at 2 months of age. NF-M$^{S\rightarrow E/S\rightarrow E}$ mice had a significantly higher rate of falls (A) and foot slips (B) compared to wild type controls. In average, NF-M$^{S\rightarrow E/S\rightarrow E}$ mice spent less time walking (C) and walked for a significantly shorter distance (D) than wild type controls. The time walking (C), walking speed (E) and the latency to fall (F) were not different in NF-M$^{S\rightarrow E/S\rightarrow E}$ compared to NF-M$^{wt/wt}$. All observations were averaged for each genotype and analyzed for statistical significance by Student's *t*-test. *, $p < 0.05$. Error bars = SEM. $N \geq 13$. (G) There was no difference in response to heat stimulus in the hind paws of NF-M$^{S\rightarrow E/S\rightarrow E}$ mice and wild type. (H) Additionally, no difference was detected in response threshold to mechanical stimulus in front or hind paws of NF-M$^{S\rightarrow E/S\rightarrow E}$ mice compared to wild type controls. Response to noxious heat (G) was averaged for each genotype by combining both hind paws measurements and analyzed for statistical significance by a Student's *t*-test. (n = 8). Response threshold to mechanical stimulus (H) was averaged for each individual paw and analyzed for statistical significance by Student's *t*-test. (n = 8). Error bars = SEM.